Nalu-Acoustics: A GPU-Accelerated High-Order Finite-Difference Solver for Acoustic Propagation with Application to Offshore Wind Farm Noise

Eunkuk Son[1], Seungjin Kang[1], Jinjae Lee[1], Songjune Lee[1], Yun-Ho Seo[2]

[1] *Wind Energy Research Department, Jeju Global Research Center (JGRC), Korea Institute of Energy Research, 200, Haemajihaean-ro, Gujwa-eup, 63357 Jeju-si, Jeju-do, Republic of Korea*
[2] *Ax Convergence Research Center, Virtual Engineering Platform Division, Korea Institute of Machinery & Materials, 34103 Daejeon, Korea*

Abstract

This study presents Nalu-Acoustics, a GPU-accelerated high-order finite-difference solver for acoustic propagation analysis over large domains. The solver employs dispersion-relation-preserving (DRP) spatial discretization and low-dissipation low-dispersion Runge–Kutta (LDDRK) time integration to minimize numerical dispersion and dissipation. Perfectly matched layers (PML) are applied at domain boundaries to suppress spurious reflections and reduce the computational domain size. The solver is implemented in CUDA with multi-GPU support via domain decomposition, currently utilizing up to eight GPUs. A single-GPU configuration achieved an 11-fold speedup over the equivalent CPU implementation. To validate the solver, the authors conducted transmission loss measurements in shallow waters near the Southwest Offshore Wind Farm demonstration site. Over the 100–1000 Hz one-third octave bands, the predicted transmission loss agreed with the measurements within a mean deviation of 1.0 dB, comparable to the measurement standard deviation. The validated solver was applied to noise propagation from the 20-turbine demonstration site, using source data from an offshore wind turbine at rated power. The simulation resolved multi-source interference and reflection at the sea surface and seabed. The results indicate that Nalu-Acoustics can be used to estimate noise impact zones around offshore wind farms and to support environmental assessment of underwater noise exposure to marine life.

Corresponding author: *eunkuk.son@kier.re.kr.*

Keywords: *Nalu-Acoustics, Wind Farm Noise, Sound Propagation*

1. Introduction

1.1. Background

Global cumulative wind power capacity has surpassed 1 TW, and offshore wind—driven by the trend toward larger turbines and larger farms—has become one of the fastest-growing sources of renewable energy [1]. With this expansion, however, the underwater noise generated during the construction and operation of offshore wind farms has emerged as a major environmental concern due to its potential effects on marine mammals, fish, and other components of the marine ecosystem [2]. Regulatory frameworks for the quantitative management of underwater noise, such as Descriptor 11 of the EU Marine Strategy Framework Directive (MSFD), are also being strengthened [3].
The noise sources of an offshore wind turbine can be broadly divided into aerodynamic sources associated with the flow field around the blades and structure-borne sources originating from the machinery inside the nacelle. Airborne aerodynamic noise does not readily penetrate into the water because of the impedance mismatch at the air–sea interface. In contrast, vibrations generated by rotating machinery such as the gearbox and generator are transmitted through the tower and substructure and radiated into the water, and numerous field measurements have confirmed that this structure-borne path constitutes the dominant component of operational underwater noise [4][5][6]. As turbines grow beyond the 10 MW class, the radiated power of operational noise is also expected to increase [7],

making farm-scale underwater noise prediction increasingly important.

1.2. Previous Work and Limitations

Most offshore wind turbines are installed in shallow water, where acoustic propagation is a highly complex problem involving multiple reflections from the sea surface and seabed, absorption by the bottom sediments, and scattering by structures[8]. Underwater acoustic propagation has traditionally been analyzed using empirical formulas, ray tracing [9], and parabolic equation (PE) methods [10]. Ray-based methods, however, cannot accurately describe diffraction and modal interference under low-frequency, shallow-water conditions, while PE-based methods—owing to their far-field approximation and one-way propagation assumption—are difficult to apply to farm-scale problems involving mutual interference among multiple sources and backscattering [8][11]. Moreover, none of these methods is well suited to integrated near-field/far-field analyses that include structure–fluid coupled sources [7].

Time-domain discretization methods have attracted attention as an alternative, but three-dimensional large-scale applications remain scarce because the number of grid points grows in proportion to the domain volume. In particular, with standard low-order schemes, numerical dispersion and dissipation errors accumulate with propagation distance and with the number of points per wavelength (PPW), severely degrading the accuracy of long-range propagation analyses. In computational aeroacoustics (CAA), the dispersion-relation-preserving (DRP) finite difference scheme [12] and the low-dissipation and low-dispersion Runge–Kutta (LDDRK) time integration scheme [13]were developed to address this issue, and their effectiveness for long-range propagation problems has been demonstrated. In addition, the perfectly matched layer (PML) boundary condition [14], formulated in a stable form for the linearized Euler equations (LEE) [15], eliminates non-physical numerical reflections at the boundaries of a truncated domain, providing the basis for time-domain analysis of open-domain propagation problems.

Meanwhile, offshore wind farms are typically designed with turbine spacings of at least seven rotor diameters (7D) to avoid power losses due to wake interference[16], so a farm of 20 turbines occupies an area of several kilometers on each side. Discretizing this entire domain under non-dispersive, non-dissipative conditions (PPW $\geq$ 10) requires hundreds of millions of grid points or more, which is practically infeasible on a single processor. Recent advances in GPU computing performance and in the implementation of finite difference stencil operations on GPUs [17], together with reported multi-GPU parallelizations of wave propagation solvers at large grid scales [18], offer a realistic path toward farm-scale underwater noise propagation analysis.

1.3. Objectives and Outline

This paper presents a method for analyzing the underwater noise impact range of an offshore wind farm that accounts for both multiple reflections in a shallow-water waveguide and mutual propagation interference among turbines. To this end, (i) the DRP spatial discretization scheme [12] and the LDDRK time integration scheme [13], which possess non-dispersive and non-dissipative numerical properties, are applied to the LEE; (ii) the PML boundary condition [15] is imposed on the outer boundary of the farm domain to block the inflow of numerical reflections without excessively enlarging the computational domain; and (iii) a CUDA-based multi-GPU parallel computing framework is developed to enable large-scale analysis of a full-scale farm layout with 20 turbines. The remainder of this paper is organized as follows. Section 2 describes the governing equations and numerical schemes, Section 3 presents the multi-GPU implementation and its verification, Section 4 reports the analysis results for the 20-turbine farm and the assessment of the noise impact range, and Section 5 concludes the paper.

2. Numerical Implementation

2.1. Governing Equations

To describe sound propagation in a moving inhomogeneous medium, this study adopts the two-equation set derived by Ostashev et al. [19] as the governing equations. The coupled equations for the acoustic pressure p and the acoustic velocity $\mathbf{w}$ are

$$\left(\frac{\partial}{\partial t} + \mathbf{v}\cdot\nabla\right)p + \varrho c^2\,\nabla\cdot\mathbf{w} = \varrho c^2 Q \tag{1}$$

$$\left(\frac{\partial}{\partial t} + \mathbf{v}\cdot\nabla\right)\mathbf{w} + (\mathbf{w}\cdot\nabla)\mathbf{v} + \frac{\nabla p}{\varrho} = \mathbf{F}/\varrho \tag{2}$$

where c is the sound speed, ϱ is the ambient density, $\mathbf{v}$ is the ambient flow, and Q and $\mathbf{F}$ are source terms representing mass injection and external force, respectively. The advective derivative operator $(\partial/\partial t + \mathbf{v}\cdot\nabla)$ denotes the time rate of change observed following a fluid particle carried by the ambient flow. In particular, the term $(\mathbf{w}\cdot\nabla)\mathbf{v}$ in Eq. (2), although the equation is a linearized momentum equation, accounts for the refraction and distortion of the acoustic velocity field by the spatial shear of the ambient flow; this term reflects the physical mechanisms of upwind/downwind refraction asymmetry and shadow-zone formation.

Since Eqs. (1) and (2) are first order in time, they are suitable for explicit time-marching, and the required input fields are only c, ϱ, and $\mathbf{v}$. These properties make the equation set an appropriate starting point for FDTD-based sound propagation analysis. However, the second-order staggered-grid FDTD scheme presented in the original paper [19][20] accumulates numerical dispersion and dissipation errors unless a sufficient number of grid points per wavelength is used, making it difficult to preserve the non-dispersive and non-dissipative nature of acoustic waves over long propagation distances. In this study, the dispersion-relation-preserving (DRP) scheme of Tam and Webb [12] is therefore employed for spatial differencing, and the low-dissipation and low-dispersion Runge–Kutta (LDDRK) scheme of Hu et al. [13] is employed for time integration.

2.2. Conservative Form of the Governing Equations

To apply the DRP differencing and the LDDRK time integration, Eqs. (1) and (2) are rewritten as a conservative vector equation for the state vector:

$$\frac{\partial \mathbf{U}}{\partial t} + \frac{\partial \mathbf{F}_x}{\partial x} + \frac{\partial \mathbf{F}_y}{\partial y} + \frac{\partial \mathbf{F}_z}{\partial z} = \mathbf{S} \tag{3}$$

$$\mathbf{U} = (p', \, w_x, \, w_y, \, w_z)^{\mathrm{T}}, \qquad \mathbf{F}_x = \mathbf{AU}, \quad \mathbf{F}_y = \mathbf{BU}, \quad \mathbf{F}_z = \mathbf{CU} \tag{4}$$

The flux matrices $\mathbf{A}$, $\mathbf{B}$, and $\mathbf{C}$ are variable-coefficient matrices composed of the ambient fields c, ϱ, and $\mathbf{v}$. The source term $\mathbf{S}$ includes the external acoustic source, the coupling terms due to the ambient flow shear, and the PML damping terms.

2.3. Spatial Differencing: DRP Scheme

The DRP scheme [12] is an optimized finite-difference method in which the coefficients of a central-difference stencil are determined by a dispersion-relation-preserving condition in wavenumber space rather than by the order conditions of a Taylor expansion, so that the physical dispersion relation is accurately reproduced over a wide range of wavenumbers. The first spatial derivative is approximated by an antisymmetric central difference on a seven-point stencil:

$$\left.\frac{\partial f}{\partial x}\right|_i \approx \frac{1}{\Delta x} \sum_{j=-3}^{3} a_j \, f_{i+j} \tag{5}$$

The coefficients a_j are determined by minimizing the integrated error between the modified wavenumber $\bar{\alpha}\Delta x$ and the exact wavenumber $\alpha \Delta x$ [12]. As a result, the scheme resolves a wider range of wavenumbers on a given grid than the standard sixth-order central difference.

2.4. Time Integration: LDDRK Scheme

Time integration is performed with the five-stage LDDRK scheme optimized for acoustic computations by Hu et al. [13]. By optimizing the amplification factor in wavenumber–frequency space, the scheme provides the following properties compared with conventional Runge–Kutta methods:
- Low dissipation: minimized numerical amplitude damping
- Low dispersion: minimized numerical phase error

For memory efficiency, the scheme is implemented in the 2N-storage form, which requires only one auxiliary array $\boldsymbol{\delta}$ in addition to the state vector $\mathbf{u}$. At each stage $s = 0, 1, \dots, 4$, the auxiliary array and the state vector are updated sequentially:

$$\boldsymbol{\delta} \leftarrow \alpha_s \boldsymbol{\delta} + \Delta t \cdot \mathrm{RHS}(\mathbf{u}), \qquad \mathbf{u} \leftarrow \mathbf{u} + \beta_s \boldsymbol{\delta} \tag{6}$$

The time step Δt is restricted by a CFL condition that accounts for both the DRP modified wavenumber and the stability region of the LDDRK scheme.

2.5. Absorbing Boundary Condition: PML (Perfectly Matched Layer)

To absorb outgoing waves at the boundaries of the computational domain without reflection, the unsplit PML formulation of Hu [21] is applied in all directions in three dimensions. The modified governing equation in the PML region is

$$\frac{\partial \mathbf{U}}{\partial t} = \mathbf{L}(\mathbf{U}) - (\sigma_x + \sigma_y + \sigma_z)\mathbf{U} - \sigma_x \sigma_y \mathbf{q}_z - \sigma_y \sigma_z \mathbf{q}_x - \sigma_x \sigma_z \mathbf{q}_y \tag{7}$$

where $\mathbf{L}(\mathbf{U})$ is the spatial discretization operator of the interior region (DRP differencing with the flux matrices), σ_x, σ_y, and σ_z are the PML damping functions in each direction, and $\mathbf{q}_x$, $\mathbf{q}_y$, and $\mathbf{q}_z$ are auxiliary variable vectors updated by separate time-marching equations [21].

The damping coefficient follows a polynomial profile within the PML:

$$\sigma(d) = \sigma_{\max} \left(\frac{d}{D} \right)^n \tag{8}$$

where d is the distance from the interface between the interior domain and the PML ($0 \leq d \leq D$), $D = N_{\mathrm{pml}} \cdot \Delta x$ is the PML thickness, and n is the polynomial order. The maximum damping coefficient $\sigma_{\max}$ is determined from a target reflection coefficient R_0:

$$\sigma_{\max} = -\frac{(n+1)c_0 \ln R_0}{2D} \tag{9}$$

In this study, $n = 3$ and $R_0 = 10^{-5}$ are used as default values.

3. Model Validation

3.1. Field Measurements

To validate the numerical model described in the preceding sections, field measurements of frequency-dependent transmission loss were conducted and compared with numerical predictions under the same conditions. The measurements were carried out on 17 October 2025 (first campaign) and 29 October 2025 (second campaign) in coastal waters near the planned site of the Southwest Offshore Wind Farm demonstration area (Buan, Jeollabuk-do, Republic of Korea). The equipment used in the measurements and its main specifications are listed in Table 1.

Table 1: Specifications of the measurement equipment

Equipment	Specifications
Underwater sound source	Frequency range: 100 Hz – 9 kHz Maximum SPL: 196 dB re 1 µPa @ 600 Hz
Hydrophone	Depth rating: 900 m Sensitivity: −200 dBV re 1 µPa
Sound velocity profiler	Range: 1,375 – 1,900 m/s Resolution: 0.001 m/s
Ambient noise recorder	Bandwidth: 20 Hz – 150 kHz (±3 dB) Sample rates: 32 – 384 kHz
Acoustic calibrator	Calibration frequency: 251.19 ± 0.30 Hz, 1000 ± 1.00 Hz SPL: 114.0 ± 0.2 dB, 94.0 ± 0.2 dB re 20 µPa
Tide gauge	Range: 50 dbar Accuracy: ±0.05 % of full scale
GPS	Horizontal accuracy: ±(0.25 m + 1 ppm) RMS Vertical accuracy: ±(0.50 m + 1 ppm) RMS
ADCP	Velocity accuracy: ±0.3 % of water velocity Velocity range: ±5 m/s (default)

The sound source (underwater speaker) was deployed at a depth of $S_z = 10\,\mathrm{m}$, and a reference hydrophone was placed at the same depth ($H_z = 10\,\mathrm{m}$) at a distance of $D_{Ref} = 1\,\mathrm{m}$ from the source to measure the source level. Receiving hydrophones were positioned at a depth of $R_z = 10\,\mathrm{m}$ at separation distances of $D_i = 50,\ 100,\ 150,\ \text{and}\ 200\,\mathrm{m}$. The source signals were tones at 200, 500, and 1000 Hz, and each condition was measured ten times to obtain the mean and standard deviation. The sound speed profile, tide level, current velocity, and ambient noise were monitored concurrently and used as the input environmental fields for the numerical model.

3.2. Comparison Procedure

In the numerical analysis, the acoustic signal recorded at the reference hydrophone ($D_{Ref} = 1\,\mathrm{m}$) was used as the source input, and the acoustic pressure at the receiver position was predicted. Since the source signal was sustained for 10 s, the simulation was run over the same 10 s interval. The SPL at the reference and receiver positions and the transmission loss (TL) between the two positions were analyzed in one-third octave bands (100–1000 Hz). Figure 1 shows the simulated pressure field for the case with a source frequency of 200 Hz and a separation distance of 200 m.

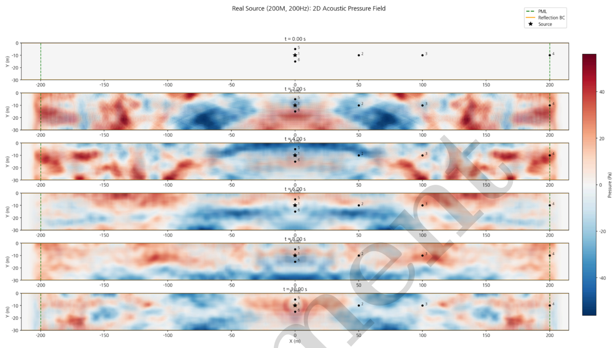

Figure 1: Simulated acoustic pressure field (source frequency 200 Hz, separation distance 200 m).

3.3. Results and Discussion

Figure 2 and Figure 3 compare the measured and predicted SPL, and the TL derived from them, in one-third octave bands for the 200 m separation case.

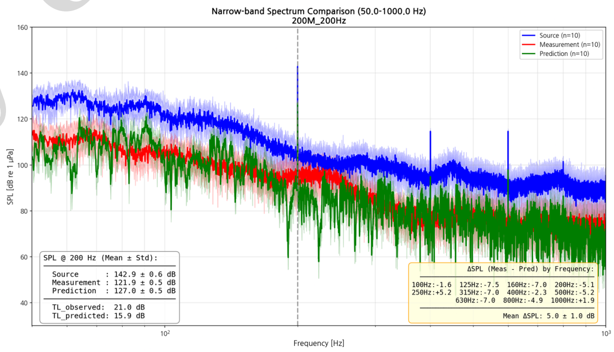

Figure 2: Comparison of measured and predicted SPL at 200 m seperation

In the SPL comparison shown in Figure 2, the predictions exceeded the measurements by 3.6 dB on average over all bands, with band-wise deviations ranging from −7.3 dB to +5.0 dB. In the TL comparison, the deviations were within 4.1 dB in all bands except the 250 Hz band, and the mean deviation over all bands was 1.0 dB. The smaller deviation in TL compared with SPL is attributed to the fact that TL is defined as the level difference between the reference and receiver positions, so that run-to-run variations in the source level cancel out. The model thus reproduces the range-dependent propagation characteristics more consistently than the absolute levels, which is the property required for the noise impact range prediction addressed in

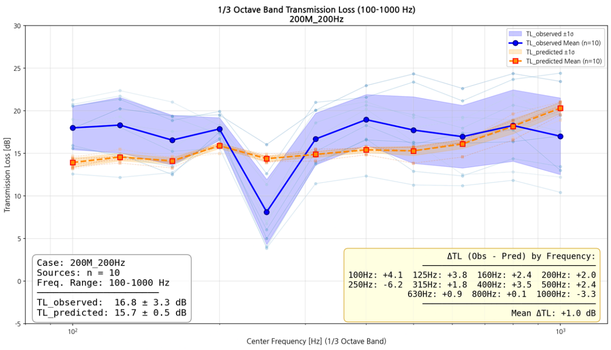

Figure 3: One-third octave band transmission loss at 200 m separation distance

Figure 3 shows that the standard deviations of the measured TL (1.3–4.5 dB) are considerably larger than those of the predicted TL (0.3–0.9 dB); since the environmental fields are fixed in the simulations, this difference reflects environmental fluctuations during the measurements, such as sea surface motion, mooring displacement, and ambient noise. The exception is the 250 Hz band, where the measured TL (8.1 dB) is markedly lower than in the adjacent bands (16–18 dB); given the large standard deviation in this band, local interference due to multipath propagation or ambient noise contamination is a probable cause, although it cannot be identified from a single receiver position.

Except for the 250 Hz band, the numerical model reproduces the measured TL in the 100–1000 Hz bands within the level of the measurement standard deviation, with a mean deviation of 1.0 dB, which supports the use of the model for the farm-scale propagation analysis in the following section.

4. Offshore Wind Farm Noise

4.1. Farm-Scale Underwater Noise Analysis

Using the numerical model validated in the preceding section, the underwater noise levels around the Southwest Offshore Wind Farm demonstration site were estimated for operation at the rated-power generation condition. The noise source input was taken from the long-term measurement data of the Gunsan offshore wind turbine, using the source signals observed during the rated-power intervals, and a time-domain underwater noise propagation simulation was performed.

The computational domain was set to 5,000 m × 4,300 m × 30 m, reflecting the layout of the 20 turbines at the demonstration site. The analysis employed approximately 1.56 billion grid points, and 138,571 time steps were advanced with a CFL number of 0.25. The computation was performed in parallel on eight GPUs and took 57 hours in total.

Figure 4 shows the simulated instantaneous acoustic pressure field over the entire computational domain. Acoustic waves radiated from each turbine propagate through the shallow-water waveguide and superpose with those radiated from neighboring turbines. The analysis thus allows the noise propagation process, including the interference among multiple sources, to be observed in the time domain over the entire farm area.

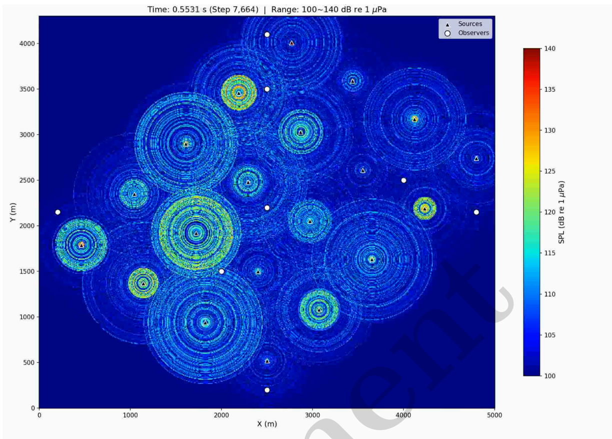

Figure 4: Simulated instantaneous acoustic pressure field over the wind farm domain (5,000 m × 4,300 m × 30 m) at the maximum power generation condition.

5. Conclusions

This paper established a farm-scale underwater noise analysis framework(Nalu-Acoustics) that combines a non-dispersive, non-dissipative time-domain scheme (DRP–LDDRK with PML) with multi-GPU parallelization, capturing both multiple reflections in the shallow-water waveguide and mutual interference among turbines. Against field transmission-loss measurements, the predictions agreed within a mean deviation of 1.0 dB—the level of the measurement standard deviation—confirming the range-dependent propagation fidelity required for noise impact range prediction.

Applying the validated model to the 20-turbine Southwest demonstration site at rated power, a computation of approximately 1.56 billion grid points was completed in 57 hours on eight GPUs, yielding the noise impact regions by level. This demonstrates that multi-source interference problems beyond the reach of ray-tracing and PE methods can be solved in the time domain at full farm scale, positioning the proposed method as a quantitative tool for environmental impact assessment and compliance with underwater noise regulations such as EU MSFD Descriptor 11. Future work will incorporate detailed seabed properties and extend the analysis to impact assessment linked to the auditory characteristics of marine species.

6. Acknowledgements

This work was supported by Korea Energy Agency (KEA) grant funded by the Korea government (MCEE) (No. RS-2025-KP900009, Development of Standardized Technology and Infrastructure for Analyzing Wind Turbine Noise Characteristics at Receptor Positions) and by Korea Institute of

Energy Technology Evaluation and Planning (KETEP) grant funded by the Korea government (MOTIE) (20220710100020, Development of layout design and underwater noise management technology for coexisting suitable offshore wind farm, and 20228520020040).

References

[1] G. W. E. C. (GWEC), "Global Wind Report 2024," *GWEC, Brussels, 2024.*, 2024.

[2] H. Bailey, K. L. Brookes, and P. M. Thompson, "Assessing environmental impacts of offshore wind farms: lessons learned and recommendations for the future," *Aquatic Biosystems*, 2014. doi: 10.1186/2046-9063-10-8.

[3] E. Parliament and C. O. T. E. Union, "Directive 2008/56/EC of the European Parliament and of the Council of 17 June 2008 establishing a framework for community action in the field of marine environmental policy," *Official Journal of the European Union, L 164, pp. 19–40*, 2008.

[4] U. N. E. F. O. W. turbines, "Underwater noise emissions from offshore wind turbines," *CFA/DAGA'04, Strasbourg, 22-25/03/2004*, 2004.

[5] T. Pangerc, P. D. Theobald, L. S. Wang, S. P. Robinson, and P. A. Lepper, "Measurement and characterisation of radiated underwater sound from a 3.6 MW monopile wind turbine," *The Journal of the Acoustical Society of America*, 2016. doi: 10.1121/1.4964824.

[6] J. Tougaard, L. Hermannsen, and P. T. Madsen, "How loud is the underwater noise from operating offshore wind turbines?," *The Journal of the Acoustical Society of America*, 2020. doi: 10.1121/10.0002453.

[7] U. Stöber and F. Thomsen, "How could operational underwater sound from future offshore wind turbines impact marine life?," *The Journal of the Acoustical Society of America*, 2021. doi: 10.1121/10.0003760.

[8] F. B. Jensen, W. A. Kuperman, M. B. Porter, and H. Schmidt, "Computational Ocean Acoustics," *Springer, New York*, 2011.

[9] M. B. Porter and H. P. Bucker, "Gaussian beam tracing for computing ocean acoustic fields," *The Journal of the Acoustical Society of America*, vol. 82, no. 4, pp. 1349–1359, 1987. doi: 10.1121/1.395269.

[10] M. D. Collins, "A split-step Padé solution for the parabolic equation method," *The Journal of the Acoustical Society of America*, vol. 93, no. 4, pp. 1736–1742, 1993. doi: 10.1121/1.406739.

[11] Y. -. Lin, T. F. Duda, and A. E. Newhall, "Three-dimensional sound propagation models using the parabolic-equation approximation and the split-step Fourier method," *Journal of Computational Acoustics*, vol. 21, no. 1, 2013. doi: 10.1142/S0218396X1250018X.

[12] Tam, C. K.W., Webb, and J. C., "Dispersion-Relation-Preserving Finite Difference Schemes for Computational Acoustics," *Journal of computational physics*, 1993. doi: 10.1006/jcph.1993.1142.

[13] F. Q. Hu, M. Y. Hussaini, and J. L. Manthey, "Low-Dissipation and Low-Dispersion Runge-Kutta Schemes for Computational Acoustics," *Journal of Computational Physics*, 1996.

[14] J. -. Bérenger, "A perfectly matched layer for the absorption of electromagnetic waves," *Journal of Computational Physics*, vol. 114, no. 2, pp. 185–200, 1994. doi: 10.1006/jcph.1994.1159.

[15] F. Q. Hu, "A stable, perfectly matched layer for linearized Euler equations in unsplit physical variables," *Journal of Computational Physics*, vol. 173, no. 2, pp. 455–480, 2001. doi: 10.1006/jcph.2001.6887.

[16] R. J. B. E. al., "Modelling and measuring flow and wind turbine wakes in large wind farms offshore," *Wind Energy*, vol. 12, no. 5, pp. 431–444, 2009. doi: 10.1002/we.348.

[17] P. Micikevicius, "3D finite difference computation on GPUs using CUDA," *in Proc. 2nd Workshop on General Purpose Processing on GPUs (GPGPU-2)*, pp. 79–84, 2009. doi: 10.1145/1513895.1513905.

[18] D. Komatitsch, G. Erlebacher, D. Göddeke, and D. Michéa, "High-order finite-element seismic wave propagation modeling with MPI on a large GPU cluster," *Journal of Computational Physics*, vol. 229, no. 20, pp. 7692–7714, 2010. doi: 10.1016/j.jcp.2010.06.024.

[19] V. E. Ostashev, D. K. Wilson, L. Liu, D. F. Aldridge, N. P. Symons, and D. Marlin, "Equations for finite-difference, time-domain simulation of sound propagation in moving inhomogeneous media and numerical implementation," *The Journal of the Acoustical Society of America*, 2004. doi: 10.1121/1.1841531.

[20] D. K. Wilson and L. Liu, "Finite-Difference, Time-Domain Simulation of Sound Propagation in a Dynamic Atmosphere," 2004.

[21] Hu and F. Q., "A Perfectly Matched Layer absorbing boundary condition for linearized Euler equations with a non-uniform mean flow," *Journal of computational physics*, 2005. doi: http://dx.doi.org/10.1016/j.jcp.2005.02.028.